CHALMERS

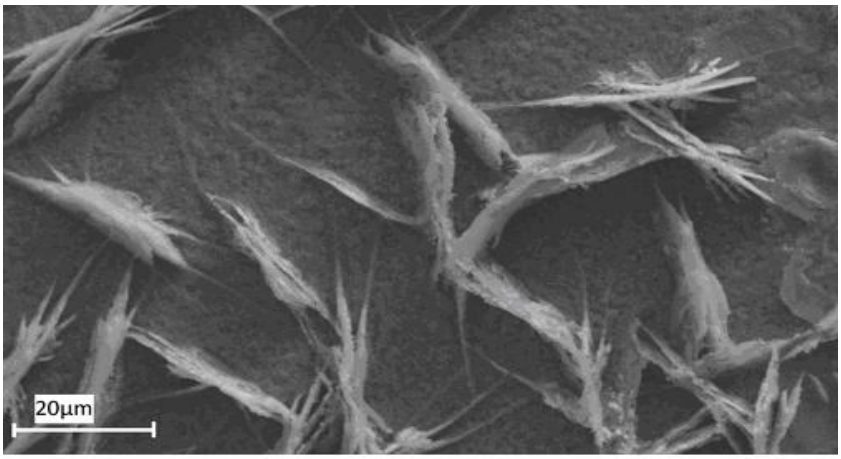

The oxidation behavior of Fe-2.25Cr-1Mo in presence of low amounts of $ZnCl_2$ at 300-400°C

Laboratory Investigations

PATRIK ÅKESSON

GUSTAF ÅLANDER

Department of Chemical and Biological Engineering

Division of Inorganic Chemistry

CHALMERS UNIVERSITY OF TECHNOLOGY

Gothenburg, Sweden, 2011

Bachelor Thesis

Report No. xxxx

The oxidation behavior of Fe-2.25Cr-1Mo in presence of low amounts of $ZnCl_2$ at 300-400°C

Laboratory Investigations

Patrik Åkesson

Gustaf Ålander

Department of Chemical and Biological Engineering

Division of Inorganic Chemistry

CHALMERS UNIVERSITY OF TECHNOLOGY

SE-412 96 Göteborg

Sweden

Telephone +46 (0)31-772 1000

Supervisors: Torbjörn Jonsson Ph. D, Erik Larsson Ph. D Student

Examiner: Professor Jan-Erik Svensson

Cover:

SEM image of Fe-2.25Cr-1Mo in presence of $ZnCl_2$ at 400°C after 24 hours of exposure.

Abstract

To reduce emissions of carbon dioxide, alternative sources for energy production have been adopted in high extent, e.g. biomass. However, since biomass contains higher concentrations of alkali metals and heavy metals compared to fossil fuels [1], corrosion problems e.g. on the waterwalls in biomass fired boilers occur in larger extent. In this work, the corrosion behavior of the low alloyed steel Fe-2.25Cr-1Mo, used in waterwalls due to its economical advantage and mechanical properties, in presence of low amounts of $ZnCl_2$ at 300 – 400°C is investigated.

Laboratory experiments were carried out in a tube furnace in wet atmosphere containing 5% O_2, 40% H_2O in N_2, with exposure times up to 168 h. Prior exposures, sample coupons were cleaned, polished, dried and deposited with 0.1 mg $ZnCl_2/cm^2$. After exposure, the coupons were analyzed with scanning electron microscopy (SEM) with energy dispersive X-ray (EDX) and X-ray diffraction (XRD).

In absence of $ZnCl_2$ at 300°C, only a very small mass gain was measured by gravimetry. In the presence of $ZnCl_2$, a local corrosion attack concentrated to the deposits was observed matching the composition of ZnO, the spinel Fe_2ZnO_4 and iron oxides. 1 and 24 h exposure yield a mass loss, partly explained by evaporation of solvent and chlorine. After 168 h, a mass gain was observed.

In absence and presence of $ZnCl_2$ at 400°C, the mass gain was considerably higher than at 300°C. In presence, no mass loss was observed, indicating faster oxidation rate.

Table of Contents

1. Introduction

The greenhouse effect partly caused by an increase of carbon dioxide, CO_2, emissions over the last 150 years to the atmosphere constitutes a global environmental problem. Therefore, national as well as international environmental agreements to minimize the dependence of fossil fuels have been adopted [2]. However, there are many factors to consider with alternative energy sources such as fuel supply, climate effects and economical factors when applying energy sources such as the sun, water, wind, nuclear or biomass than finite sources [3].

In this work, focus will be on biomass power plants which are a promising alternative in energy production with less climatic impact. Combustion of biomass causes problems with corrosion and built up deposits in the heat transferring areas in much higher extent. The main reasons why these problems occur are due to the composition of biomass, which contain higher concentrations of alkali metals and heavy metals compared to fossil fuels [4]. This results in a shortened lifetime of the process equipment like steel super heaters and water walls. To deal with this, the operating temperature may be lowered but as a result of this, the degree of efficiency is also reduced.

Earlier studies have investigated the influence of alkali chlorides at high temperatures in waste and biomass fired boilers due to significant problems with fireside corrosion. Compared to KCl, $ZnCl_2$ has a lower melt temperature which is suspected to induce corrosion at an earlier stage [5, 6].

The aim of this study is to create further understanding of the corrosion process in a biomass fired boiler which is a complex environment with many interacting species. Therefore, simplifications of the environment in a laboratory scale have been made in order to study the corrosion products induced by low amounts of $ZnCl_2$ on a low alloyed steel commonly used in biomass boiler process equipment.

2. General theory

2.1 Ferritic steel and low alloyed steel

In waste and biomass fired boilers both the costs as well as the durability of the construction materials are of great importance when designing a power plant. There are several different types of steels to choose from. High alloyed steels with high amounts of alloying elements like nickel and chromium are used to maintain the austenitic structure and improve the corrosion resistance by forming a chromium rich passive oxide layer. However, high alloyed austenitic steels are more expensive due to the high content of chromium and nickel than low alloyed ferritic steels. For this reason, ferritic steels are often considered as an alternative to stainless steels in the boiler. Furthermore, ferritic steels are mechanically stronger with higher durability and weldability than austenitic steel [7].

In this study, a low alloyed ferritic (*figure 2.1*) steel consisting of approximately 2,25 wt % chromium and 1 wt % molybdenum will be used in the experiments to investigate the ferritic properties in low temperatures to simulate a corrosion attack in the boiler. Due to the low content of chromium, a passive film of chromium oxide will not be formed. However, the mechanical properties are increased.

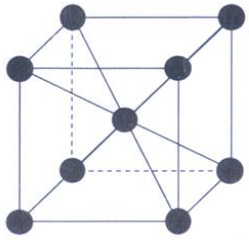

Figure 2.1. Ferritic BCC formation.

General metal properties such as bonding and structure allow other elements to be inserted into the crystal lattice. When this takes place a so called alloy is formed, but the mixture still has metallic properties. There are two types of alloys, a substitutional and interstitial alloy. Substitutional alloy is characterized by ordinary metal atoms in the lattice substitutes other metal atoms of different elements with approximately the same size. Interstitial alloy is when small atoms of another element are introduced to the vacancies in the lattice. Steel is an interstitial alloy, where carbon takes the interstitial spaces in the iron lattice. The alloy of carbon and iron results in a much stronger material compared to pure iron [8].

2.2 Defects and diffusion in oxides

In solids, e.g. oxides, there are different types of defects that allow ion transportation trough diffusion. The most fundamental defect is vacancies, which is caused by empty positions in the lattice. Another common defect is dislocations, which are line defects in the structure. There are two types of dislocations, edge- and screw dislocation. The defect in an edge dislocation is when a half-plane of atoms is located between two entire atom planes. In screw dislocation though, an atom plane is cut, which results in sharing of the halves by the surrounding atom planes. This creates a helical formation.

Grain boundary is defined as the interface between two single-crystal grains that separate surrounding crystals with different orientation creating small areas of heterogeneous lattice. [9, 10]. Within the lattice, there are three common types of diffusion; interstitial diffusion, interstitialcy diffusion and vacancy diffusion shown in *figure 2.2*. Interstitial diffusion implicates movement of ions smaller than the lattice atoms. The movement takes place in the interstitial space of the lattice. Interstitialcy diffusion implies that an atom in the lattice substituted by another atom at the time of impact between these two. In vacancy diffusion an atom changes its position to a vacant space in the lattice. Thus, the movement creates a new vacant atom position from the leaving atom [11].

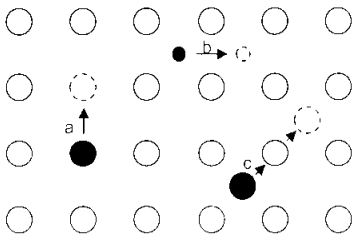

Figure 2.2. Schematic picture of a) vacancy diffusion, b) interstitial diffusion and c) interstitialcy diffusion.

2.3 Metal oxidation

Metals exposed to ambient air spontaneously oxidiates into metal oxides by the following reaction:

1. $xMe\ (s) + y½\ O_2\ (g) \rightarrow Me_xO_y\ (s)$

The reaction spontaneously occurs because it favors a change in Gibbs free energy to a lower energy level. Gibbs law of free energy at constant temperature and pressure is defined as followed:

2. $G = \Delta H - T\Delta S$

where G is Gibbs free energy of formation, H is the enthalpy change, T is the temperature in Kelvin and S is the change of entropy. The oxidation reaction takes place if $\Delta G < 0$, hence it is thermodynamically possible. In this case, the equation of Gibbs free energy can be written as followed:

3. $$\Delta G = G_{M_xO_y} - xG_M - \frac{1}{2}G_{O_2} = \Delta G^\circ + RTln(\frac{a_{M_xO_y}}{a_{Me^x * a_{O_2}^{\frac{y}{2}}}})$$

where R is the gas constant, ΔG° is the change in free energy for the species in their standard states. In its standard state, a pure solid or liquid has a thermodynamic activity equals to 1 (a in the equation above). For the oxygen the activity is equal to the partial pressure. However, this is only valid at low pressure. An oxide layer is formed if the partial pressure of the ambient oxygen is higher than the dissociation pressure of oxygen in the forming oxide [12].

2.4 Formation of protective and non protective oxides

Oxide formation starts with adsorption of oxygen molecules to the metal surface, which constitutes the very core of the oxide. Subsequently, the growth of the oxide continuous horizontally in all directions when even more oxygen is dissolved over the metal surface that results in fully oxide covered metal area (*figure 2.3*). Vertical growth of the oxide continuous until the thickness of oxide layer prevents further transportation of ions and electrons through the oxide. The only possibility to continued oxidation depends on the defects in the oxide lattice, creating pathways for ions and electron transportation [13, 14].

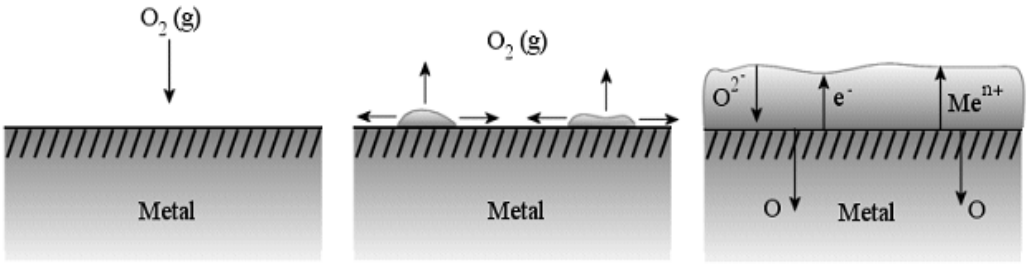

Figure 2.3. Pictures showing the process of oxide growth.

The properties of the oxide film determine whether it is protective or not. Depending on the composition of the alloy, different oxides are formed. In order for stainless steel to be protective, the oxide layer must remain coherent and adherent to the metal surface. The oxidation rate is controlled by the diffusion of metal and/or oxygen through the film. To be protective the oxide film has to be relatively impermeable under high temperatures to the reacting spices. Characterization of a non protective oxide layer is when a volume difference between the metal and the oxide that is forming. Subsequently, the oxide layer may crack and flake off which leads to a fast corrosion at the unprotected metal areas [15].

2.5 Kinetics of oxidation

By using gravimetry, which is the mass change over time, the kinetics of the oxide process can be determined. The growth can be described by three common mathematical expressions. However, these equations only describe ideal theoretical conditions under which the oxidation occurs, but are nevertheless useful for the understanding of the oxidation process.

The first equation to describe the oxidation process is the linear expression. See *equation 4*.

4. $x=k_1t + A$

where x is the thickness of the oxide, k_1 the linear rate constant, t the time and A a constant (start thickness of the oxide). This rate law illustrates an oxide growth where the thickness of the oxide is direct related (linear) to the time of exposure.

The second mathematical model to describe the kinetics of the growth of an oxide layer is the parabolic equation. See *equation 5*.

5. $x^2 = 2k_pt + D$

where x is the oxide thickness, k_p the parabolic rate constant, t is the time and D the integration constant (start thickness of the oxide) [16].

The equation formed by Wagner is suitable for oxide growth at high temperatures. Under these circumstances the rate of the oxide growth depends on how fast species diffuse through the oxide. For the Wagner theory to be valid, some premises have to be fulfilled.

i. The oxide layer must remain coherent and adherent to the metal surface.
ii. The thickness of the oxide layer is constant all over the metal substrate and is isotropic stable.
iii. The diffusion occurs mainly through lattice defects [17].

At high temperature corrosion, the parabolic expression is the most common. The characteristic behavior starts at a rather fast oxidation rate. The thicker the oxide becomes, the more the oxidation rate declines.

The third expression to be defined is the logarithmic rate law. The expression can be described either inverse or direct. See *equation 6 and 7*.

6. $\frac{1}{x} = C - k_{il} logt \ (inverse\ rate\ law)$

7. $x = k_{log} \log(t + t_0) + B \ (direct\ logharitmic\ rate\ law)$

where x is the oxide thickness, C and B are constants, k_{log} and k_{il} are rate constants and t is time of exposure. These mathematical models are suitable for describing oxide growth for temperatures under 400°C [18]. See *figure 2.4* for illustration of the three common rate laws.

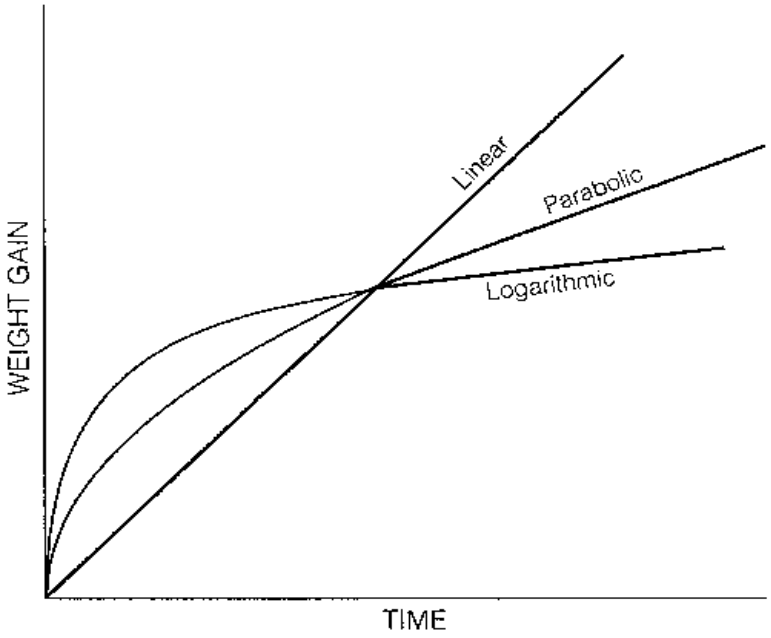

Figure 2.4. Illustration of the three corrosion rate laws.

2.6 Corrosion products

In biomass fired boilers, the built up deposits at the waterwalls consist of several species, hence forming a complex environment. In order to investigate and create understanding of different elements and their specific influence of the corrosion, simplifications of the system have to be made.

In this study, the corrosive influence of $ZnCl_2$ on the low alloyed ferritic steel Fe-2.25Cr-1Mo (T22) has been investigated. The expected oxide to be formed by $ZnCl_2$ is ZnO. The oxides formed from the steel are expected to be an iron chromium spinel type, $(Fe,Cr)_3O_4$, at the inner layer. The composition of the inner spinel may differ depending on the steel composition. The iron oxide layer may also consist of a middle layer of magnetite, Fe_3O_4. An outer layer is of hematite, Fe_2O_3 is also expected. Depending of temperature and kinetics, different proportions of magnetite and hematite are formed.

Compared to stainless steel with a higher content of chromium, the corrosion resistance of ferritic steel is much lower. However, it is often used in process equipment with relative low operating temperatures, hence the corrosion rate levels off with declining temperature, since it is a much more cost effective material and thus creates a protective oxide scale at moderate temperatures [19].

2.6.1 Origin and corrosive effects of $ZnCl_2$ in waste and biomass fired boilers

Zinc is naturally present in biomass, such as spruce and works as a nutrient. Also chlorine is naturally represented in biomass. In waste, zinc originates from for example plastics, where it is an additive to increase the properties of the material. Unsorted waste as waste wood may also contain some pieces of metal and paint in which zinc can be present. Chlorine in waste mainly derives from chlorinated plastics (about 90%) but is also released from food leftovers which contain dietary salt (NaCl).

Earlier studies have investigated the influence of KCl at high temperatures in waste and biomass fired boilers due to significant problems with corrosion at the fireside steel in the super heaters. In contrary to alkali chlorides such as KCl that has a melting point at 770°C, $ZnCl_2$ has a much lower melting point at 283°C [20], which is expected to induce corrosion on the waterwalls in the boiler that has approximately the same operating temperature as the melting point of $ZnCl_2$. When the $ZnCl_2$ is in melt the corrosion attack increases compared to solid state due to the faster ion transportation in the melt [21, 22].

3. Experimental techniques

The aim of this study is to investigate the corrosion behavior of a low alloyed steel in the presence of $ZnCl_2$ at 300 – 400°C. Therefore, laboratory studies have been performed by isothermal furnace exposures. To investigate the morphology of the corrosion products at the sample surface and the composition of the products, the analytical techniques Scanning Electron Microscopy (SEM) with Energy Dispersive X-ray (EDX) detector and X-ray Diffraction (XRD) were used.

3.1 Sample preparation

The ferritic low alloyed steel Fe-2.25Cr-1Mo used in this study was cut in pieces of 15x15x2 mm. The composition of Fe-2.25Cr-1Mo is given in *Table 1*. A hole with a diameter of 1.5 mm was drilled to be able to hang the samples during the spraying of the $ZnCl_2$ solution on the sample coupons. Thereafter, the samples were grinded and polished in several steps (9 µm, 3 µm, 1 µm diamond suspension) to obtain a shiny surface. To remove the grease from the surface, acetone were used with ultrasonic agitation. To further clean the samples, the same cleaning procedure was done but this time with ethanol. All samples were dried with cool air to dry of the solvent and stored in a desiccator to prevent atmospheric corrosion.

Table 1. Elemental composition of Fe-2.25Cr-1Mo. Concentrations in weight percent [23].

	Fe	Cr	Mo	Mn	C	P	S
Fe-2.25Cr-1Mo	96.01	2.19	0.93	0.49	0.095	0.014	0.01

3.1.1 Depositing samples with $ZnCl_2$

Solid $ZnCl_2$ is highly hygroscopic compared with for example KCl. Therefore, it is important to belay all sample coupons in systematic order to achieve reproducible laboratory exposures. To minimize exposure to ambient atmosphere, all coupons were stored in desiccators both before and after covering with $ZnCl_2$-solution. For each exposure, a set of three coupons were sprayed with approximately the same amount of $ZnCl_2$-solution (*figure 3.1*) at one side only to minimize time of exposure to ambient atmosphere. The small differ in weight depends on the very small amounts of deposited $ZnCl_2$ on each sample. The samples were dried by cool air after the spraying.

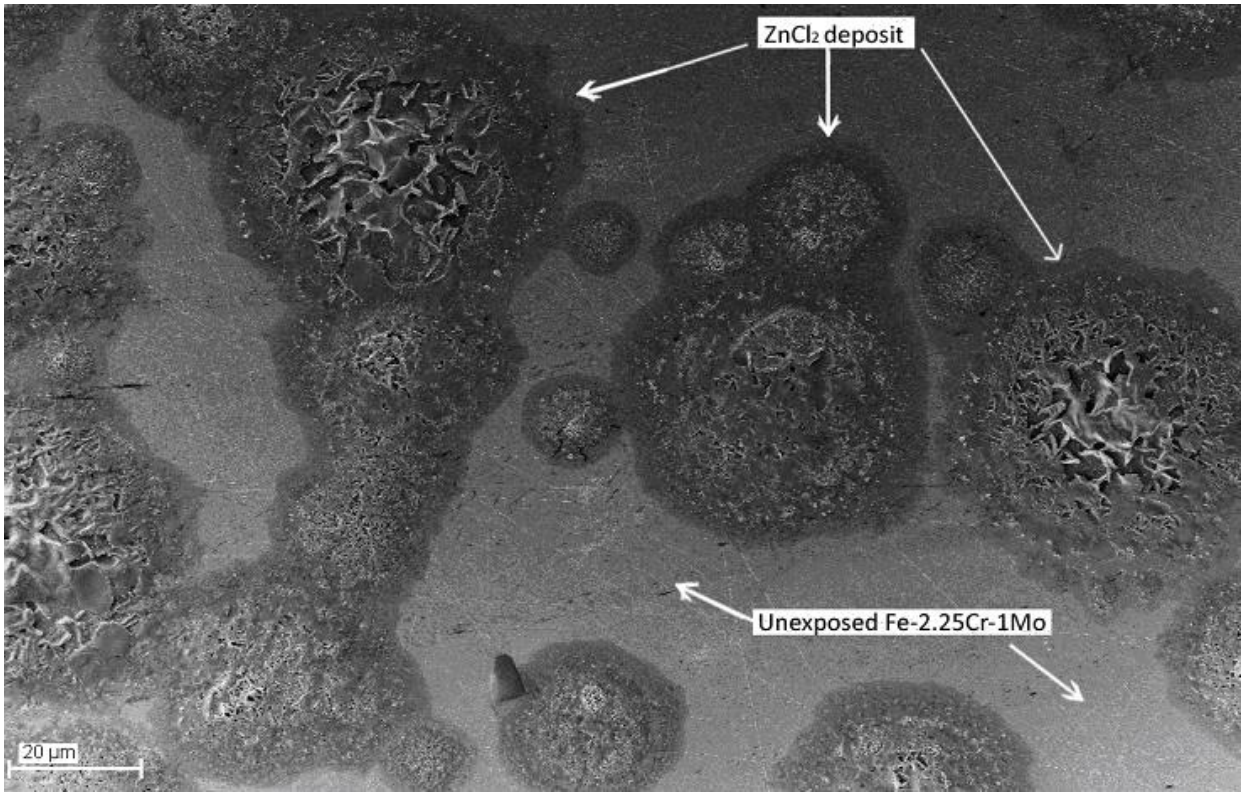

Figure 3.1. $ZnCl_2$ deposited on unexposed sample.

3.1.2 Oxidation of $ZnCl_2$ (l) into ZnO (s)

To be able to estimate the amount of pure $ZnCl_2$ on each sample, exposures on Au-plates were carried out, where Au serves as an inert surface. A certain amount of $ZnCl_2$-solution was sprayed on one side at the Au-plate. The solvent was dried out by cool air. To ensure no evaporation of $ZnCl_2$, the vapor pressure was calculated at 427°C (700K) and 227°C (500K). See *appendix 10.1*. At 427°C the vapor pressure was calculated to $2.56 \cdot 10^{-3}$ bar, under which evaporation is expected. At 227°C, the pressure was calculated to $2.26 \cdot 10^{-7}$ bar, which is a negligibly vapor pressure. Since no significant evaporation of $ZnCl_2$ will occur, the following equilibrium reaction is expected;

a) $ZnCl_2\ (s) + H_2O\ (g) \rightarrow ZnO\ (s) + 2HCl\ (g)$

The amount of HCl that is formed has a calculated vapor pressure of $3 \cdot 10^{-3}$ bar, which is relatively high, leading to evaporation of HCl. The $ZnCl_2$ therefore forms ZnO according to *reaction a),* that subsequently remains on the sample surface.

Due to the calculations carried out, approximately 0.1 mg/cm^2 of $ZnCl_2$ was sprayed on the sample coupons. For calculations, see *appendix 10.2*.

Under the laboratory exposures with T22 at 300, 400°C, a higher evaporation rate of $ZnCl_2$ is expected because of the higher temperature.

3.2 Exposures

To simulate an operating biomass fired boiler, the exposures were carried out in the presence of O_2 (5%) with H_2O (40%) in N_2. The sample coupons were mounted on a ceramic plate and inserted in a tube furnace (*figure 3.2*) with a diameter of 43 mm under isotherm conditions at 300 and 400°C. Between these temperatures, $ZnCl_2$ is expected to form low temperature melt. The furnaces are well isolated to keep the temperature profile as even as possible. To ensure correct exposure temperature, a thermocouple was used before each exposure. Due to variations of temperature in the furnace tube, the temperature profile was measured for both furnaces at 400°C to ensure that the sample coupons were placed at the right position. The temperature profiles are presented in *appendix 10.3*. According to the temperature profiles, the temperatures are more stable some centimeters beyond the exposure position in the furnaces. Therefore, smaller relative variations in the exposures may occur. To guarantee the correct humidity in the gas mixture passing the samples in the tube, all parts of the laboratory equipment were held at temperatures above 100°C, to prevent any condensation of H_2O. The gas flow rate during the exposures was 1000 ml/min. Exposure times during each separate experiment lasted for 1, 24 and 168 hours.

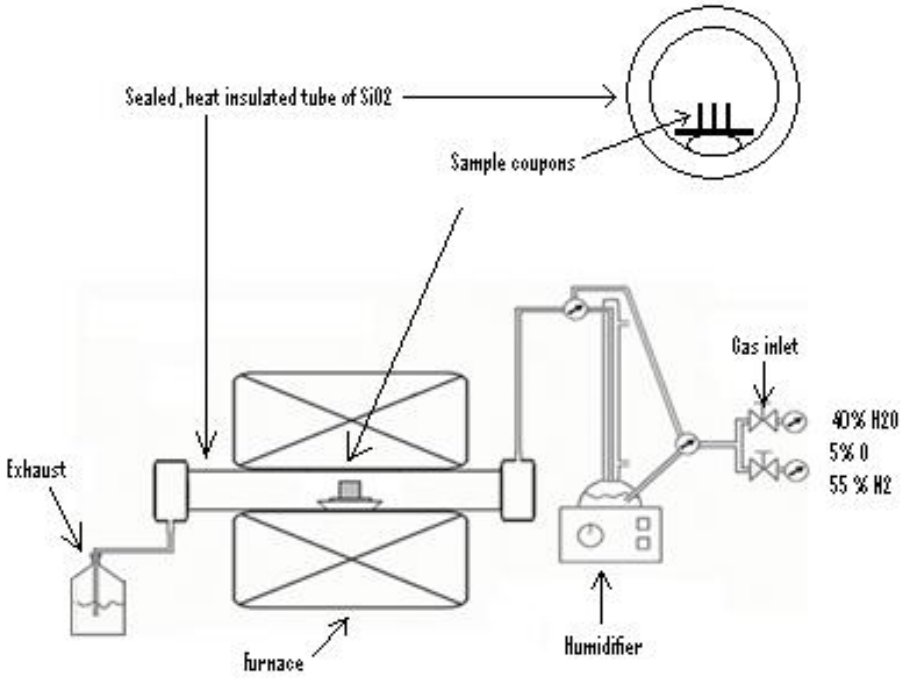

Figure 3.2. Schematic picture of laboratory equipment used for exposures of the sample coupons.

4. Analytical techniques

To analyze the corrosion attack, different analytical techniques has been used. Though the corrosion occurs at microscopic level, techniques like SEM and XRD provides valuable information, hence makes it possible to link the mass gain curves to the corrosion products.

4.1 Scanning Electron Microscopy (SEM)

Scanning electron microscopy is mainly used to analyze the morphology and composition of the corrosion products. It can also provide information about the chemical composition.

An electron gun creates a beam of electrons that passes through several electron lenses and hits the sample surface. The impact of the electron beam creates a pear shaped sphere called the interaction volume. See *figure 4.1*. From this interaction volume, several signals are generated. In this work, three types of signals were used to analyze the exposed samples. The high energy backscattered electrons provides information about the chemical composition and/or density of the sample. Depending on atom size, larger atoms reflect a higher number of electrons compared to smaller atoms. The more electrons that are detected, the brighter the measured pixel appears on the monitor. Secondary electrons have a much lower energy than backscattered electrons and are used to obtain pictures with high resolution. Chemical composition can also be provided by detecting X-rays in an EDX-detector attached to the SEM [24].

The SEM used in this study was equipped with an EDX-detector and operated in high vacuum mode at an acceleration voltage of 15kV.

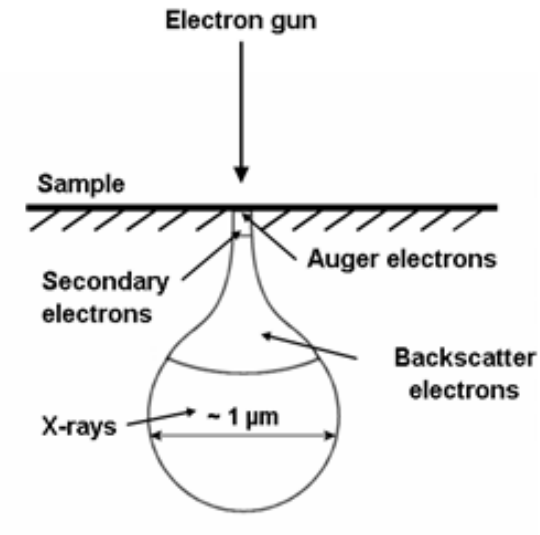

Figure 4.1. Schematic picture of the interaction volume as the electron beam strikes the sample surface.

4.2 X-Ray Diffraction (XRD)

X-ray diffraction is an analysis method for detecting crystalline solids. The diffraction occurs when an X-ray beam interacts with the crystal and is scattered by deflection from the intended path. When two parallel X-rays strike the lattice at the same angle, the first X-ray strikes the first atom and is reflected, while the second X-ray strikes the second layer in the lattice and is reflected by that (*figure 4.2*), the difference in the travelled distance after reflection is an integral number of wavelengths. Since there is a correlation between distance travelled after reflection and spacing between the layers in the lattice, Bragg's law is applied.

8. $2d_{hkl} . sin\Theta = n\lambda$

where d is the distance between the atoms and Θ is the angle of incidence and reflection, *n* is a integral number and λ is the wavelength of the X-rays. A given structure, e.g. Fe_2O_3, gives a number of peaks in a diagram. These peaks can be compared with a database and identified [24, 25].

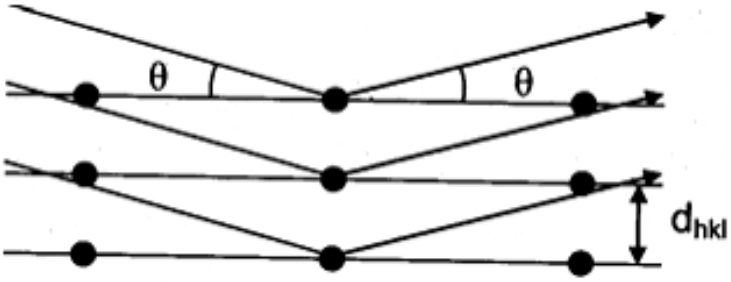

Figure 4.2. X-rays striking the metal lattice at the angle Θ

5. Results

5.1 Morphology of unexposed Fe-2.25Cr-1Mo in presence of $ZnCl_2$

Figure 5.1 shows the morphology of an unexposed sample deposited by $ZnCl_2$ solution. No single salt crystals are observed in contrast to e.g. KCl deposits (*see figure 5.2*). However, $ZnCl_2$ crystals mixed with solvent in bulky formations can be observed. In between the $ZnCl_2$ deposits, pure Fe-2.25Cr-1Mo surface is seen.

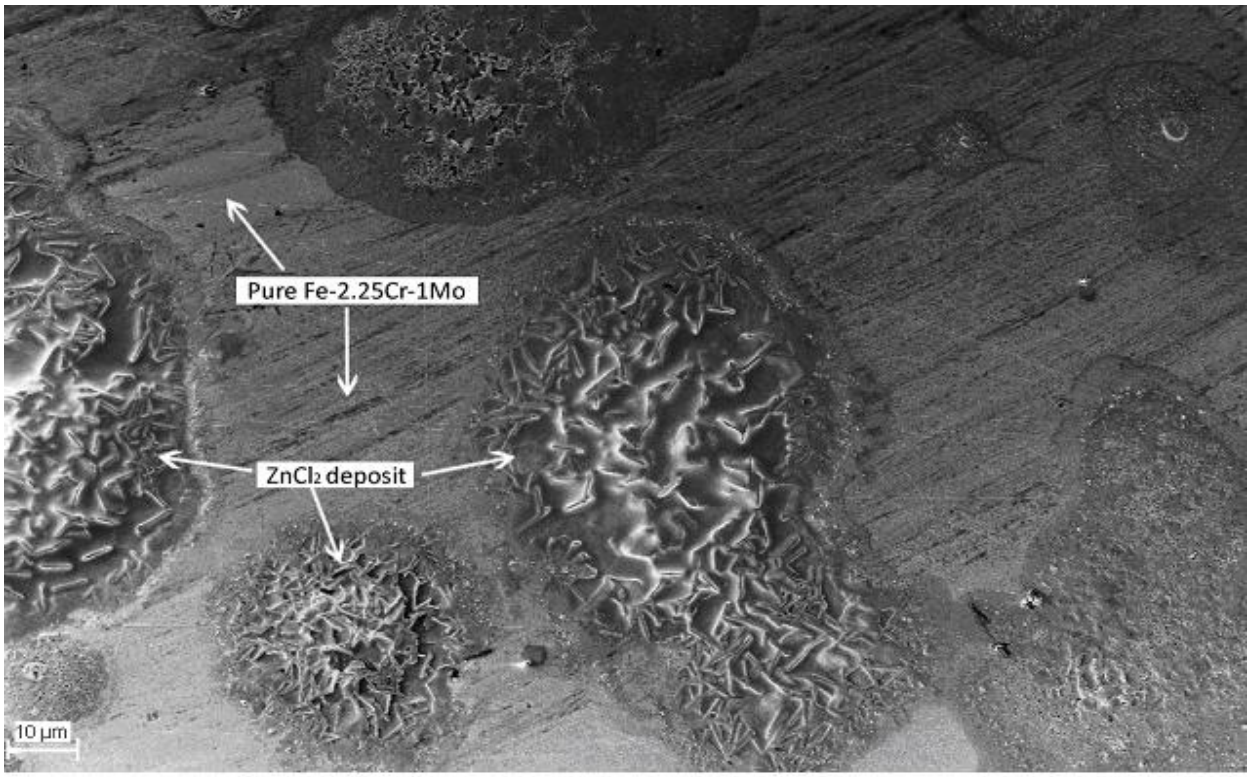

Figure 5.1. Morphology of $ZnCl_2$ deposition on uexposed Fe-2.25Cr-1Mo.

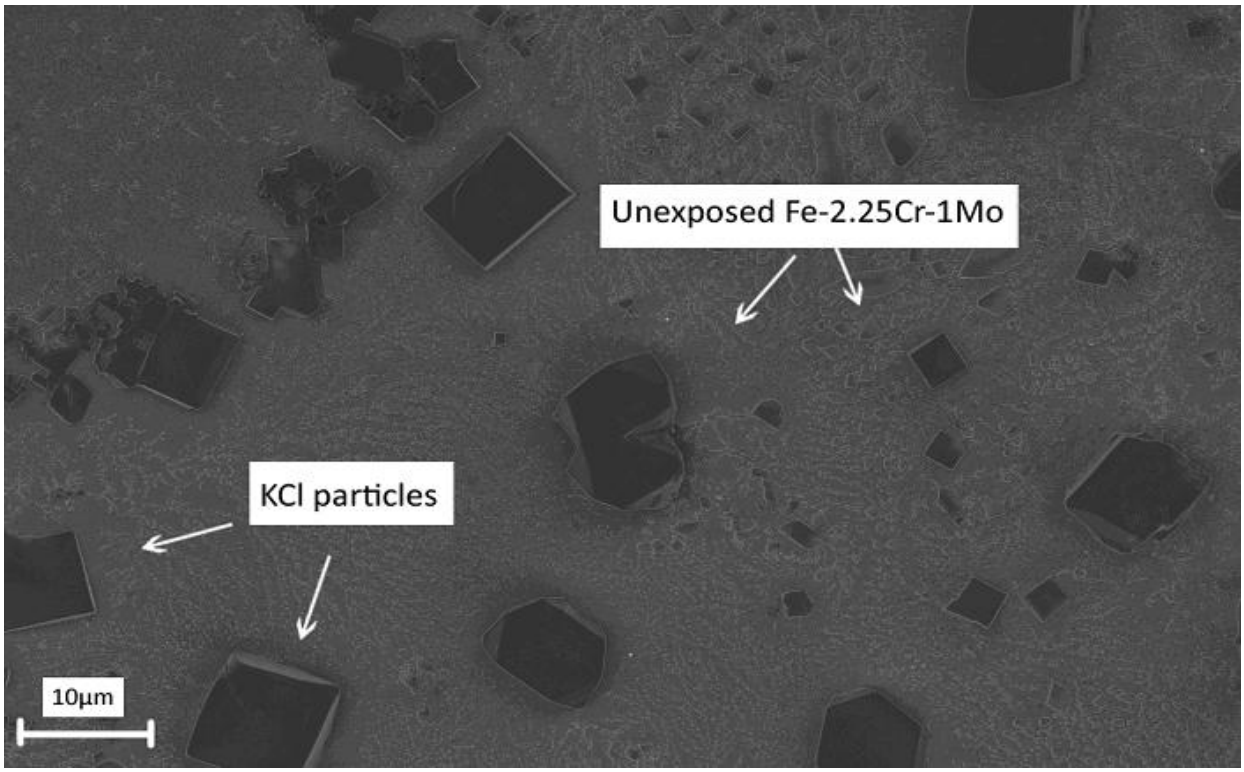

Figure 5.2. Morphology of KCl deposition on uexposed Fe-2.25Cr-1Mo.

5.2 Oxidation of Fe-2.25Cr-1Mo in presence and absence of $ZnCl_2$ at 300 °C

5.2.1 Mass change

Figure 5.3 shows mass gain up to 168 hours in presence and absence of $ZnCl_2$ of Fe-2.25Cr-1Mo (T22). During reference exposures at 300°C, without $ZnCl_2$, only a very small mass gain could be observed. The oxidation is somewhat faster during the first 24 hours. Thereafter, the slope levels off to a lower oxidation rate.

In presence of $ZnCl_2$ (~0.1 mg/cm^2 pure $ZnCl_2$ in ~0.27 mg/cm^2 solvent), 1 hour exposure demonstrates a rapid mass loss indicating evaporation of solvent and Cl from the solution of $ZnCl_2$ deposit. After 24 hours, a smaller mass loss compared to 1 hour is observed, which indicates oxide growth. After 168 hours, the mass gain is approximately the same as for the reference.

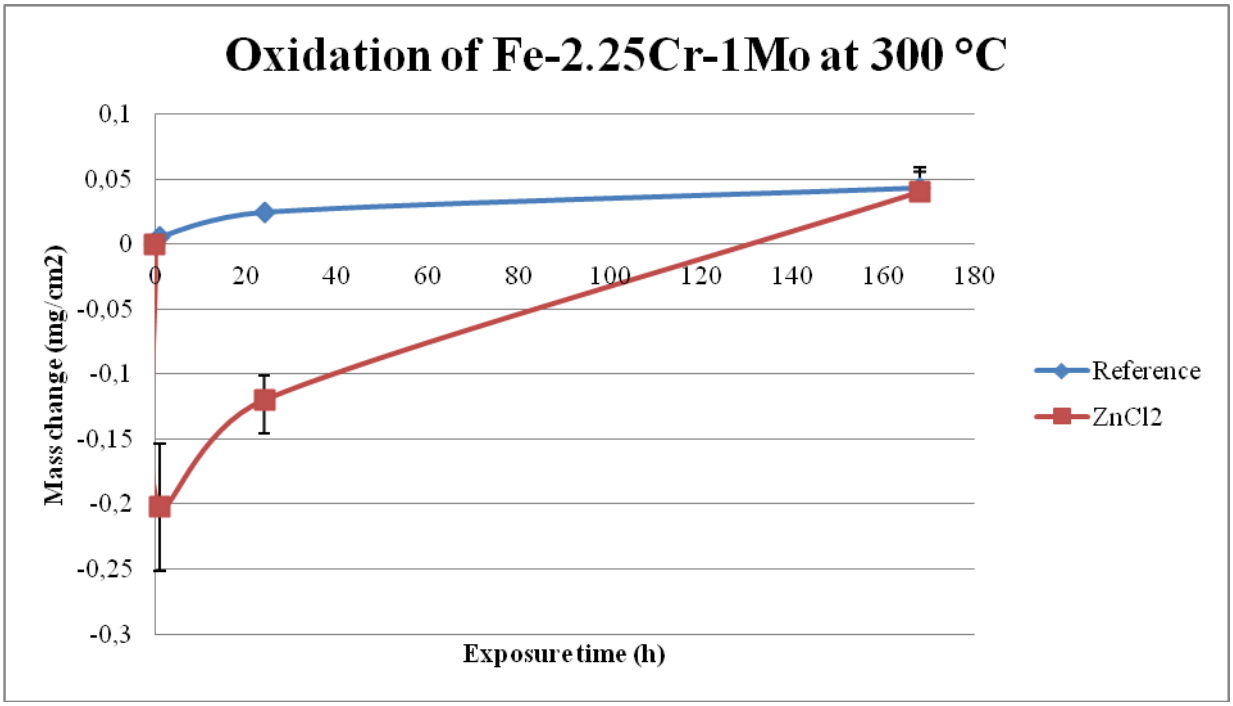

Figure 5.3. Mass change curve of Fe-2.25Cr-1Mo in both absence and presence of $ZnCl_2$.

5.2.2 Oxide morphology at 300°C

In absence of $ZnCl_2$: In addition to gravimetry, SEM with an EDX detector was used to investigate the morphology and the composition of the products. Also, XRD was used to detect crystalline solids. After reference exposures, the samples have homogenous surface morphology as seen in *figure 5.4* After 1, 24 and 168 hours reference exposure, the oxide thickness was calculated to 10, 47 and 83 nm respectively, hence, a small mass gain and a slow oxide growth even after relatively long exposure times. No signs of spallation was observed.

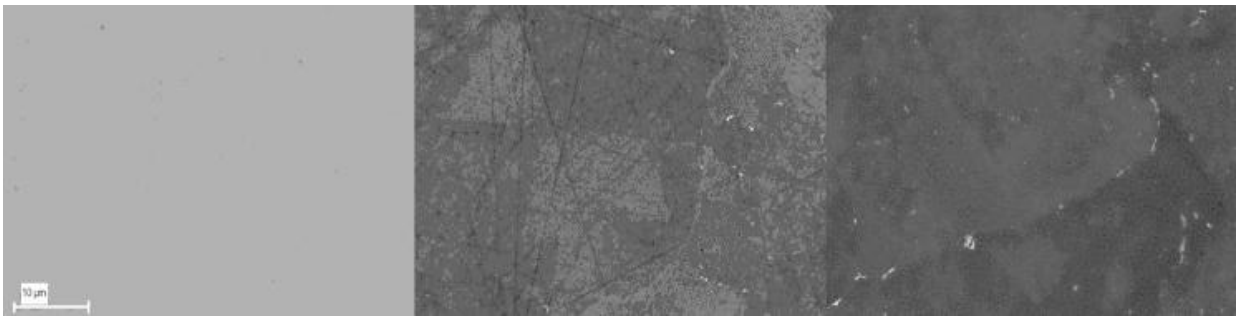

Figure 5.4. Reference exposures of Fe-2.25Cr-1Mo, 300°C, 1, 24, 168h.

In presence of $ZnCl_2$: After 1 hour at 300°C in presence of $ZnCl_2$, three features were observed, see *figure 5.4*. The base oxide thickness was estimated by interpreting EDX analysis to be below ~0.5 µm. Apart from the smooth undeposited base oxide area, mainly two types of characteristic morphologies were observed.

Detected by EDX, it is probable that the $ZnCl_2$ forms a composition consisting of ~ 30% Zn, 10 % Fe and 60% O, i.e a mixture of ZnO and iron oxide. In addition to these, a composition matching the spinel Fe_2ZnO_4 was observed. The results from EDX were matched by XRD and showed that ZnO and Fe_2ZnO_4 were formed but iron oxide amount was below the detection limit. The oxide formations were uneven distributed over the samples, probably related to the different amounts of deposit. The characteristic morphologies of oxides are shown in *figure 5.5 B and C*. Negligible amounts of Cl (~1%) were detected which indicates evaporation of Cl. At high magnification, the two types of characteristic oxide morphologies are clearly seen. The structure in *figure 5.5 B* shows similarities to the unexposed sample in *figure 5.1*. The bulky shape remains, but inside, the outlines of the inner structure are more visible since evaporation of solvent.

As seen in *figure 5.5 C*, the outlines are sharper with lower amounts of Zn, but slight higher amount of Fe according to the EDX, which could indicate a later stage of oxide formation compared to *figure 5.5 B*, where the structure reminds more of the unexposed sample in *figure 5.1*.

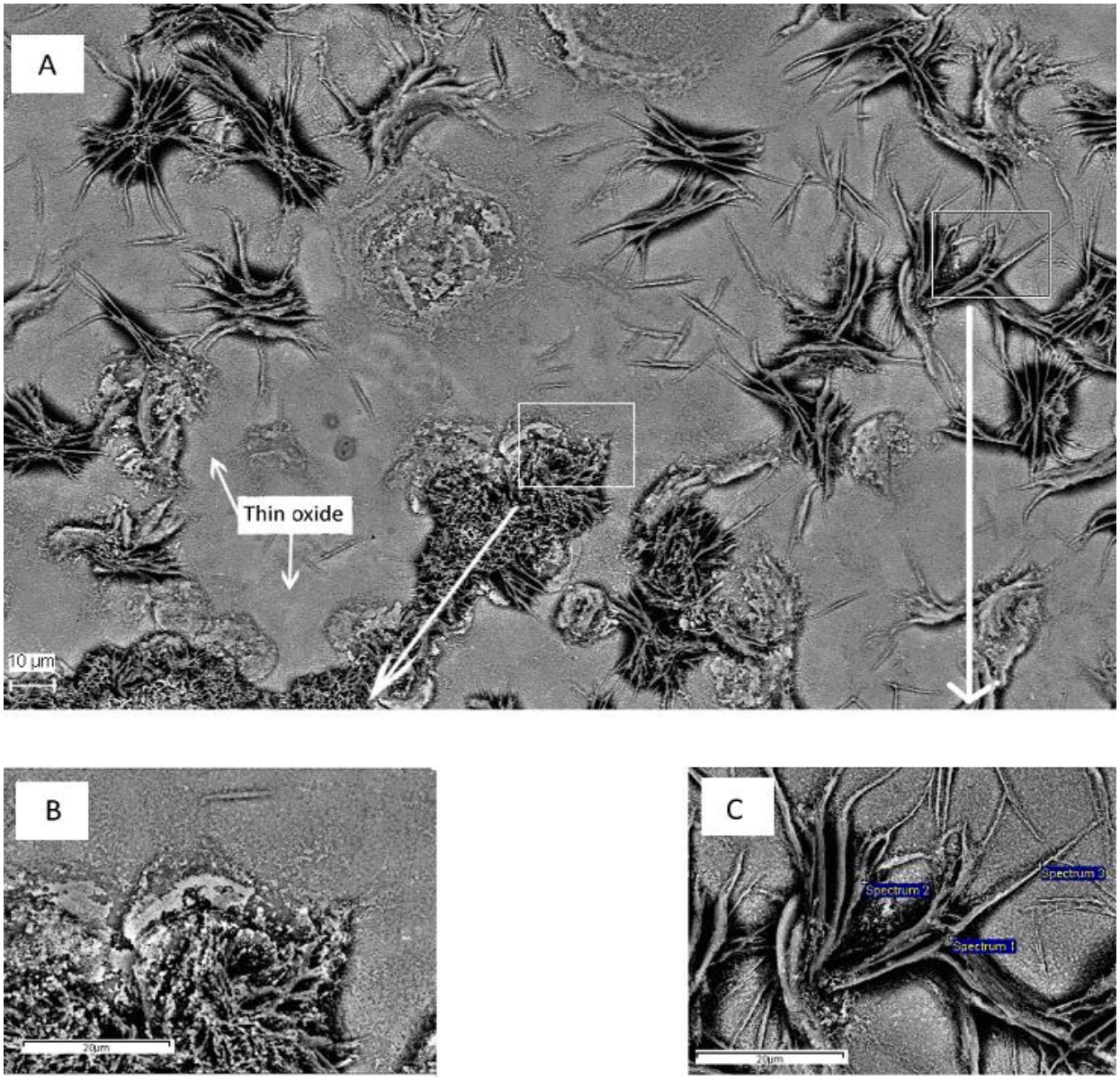

Figure 5.5. Fe-2.25Cr-1Mo in presence of $ZnCl_2$ at 300°C, 1h.

After 24 hours, there are still many similarities in surface structure with 1 hour exposure. A significant change is that there are no areas with bulky formations as after 1 hour (*figure 5.5 B*). Only sharp formations remain after 24 hours, but with different sizes. The smaller formations that may be Fe_2ZnO_4 have a typical size between 5-10 µm and the larger mixture of ZnO and

iron oxides between 20-30 µm. Due to the structure compared with the unexposed sample in *figure 5.1*, it may be assumed that the solvent has evaporated and the inner structure of the spinel becomes clearer. Furthermore, there are more small formations, with lower concentration of Zn and more Fe, than the large ones. This could depend on variations of $ZnCl_2$ deposits, i.e. starting conditions.

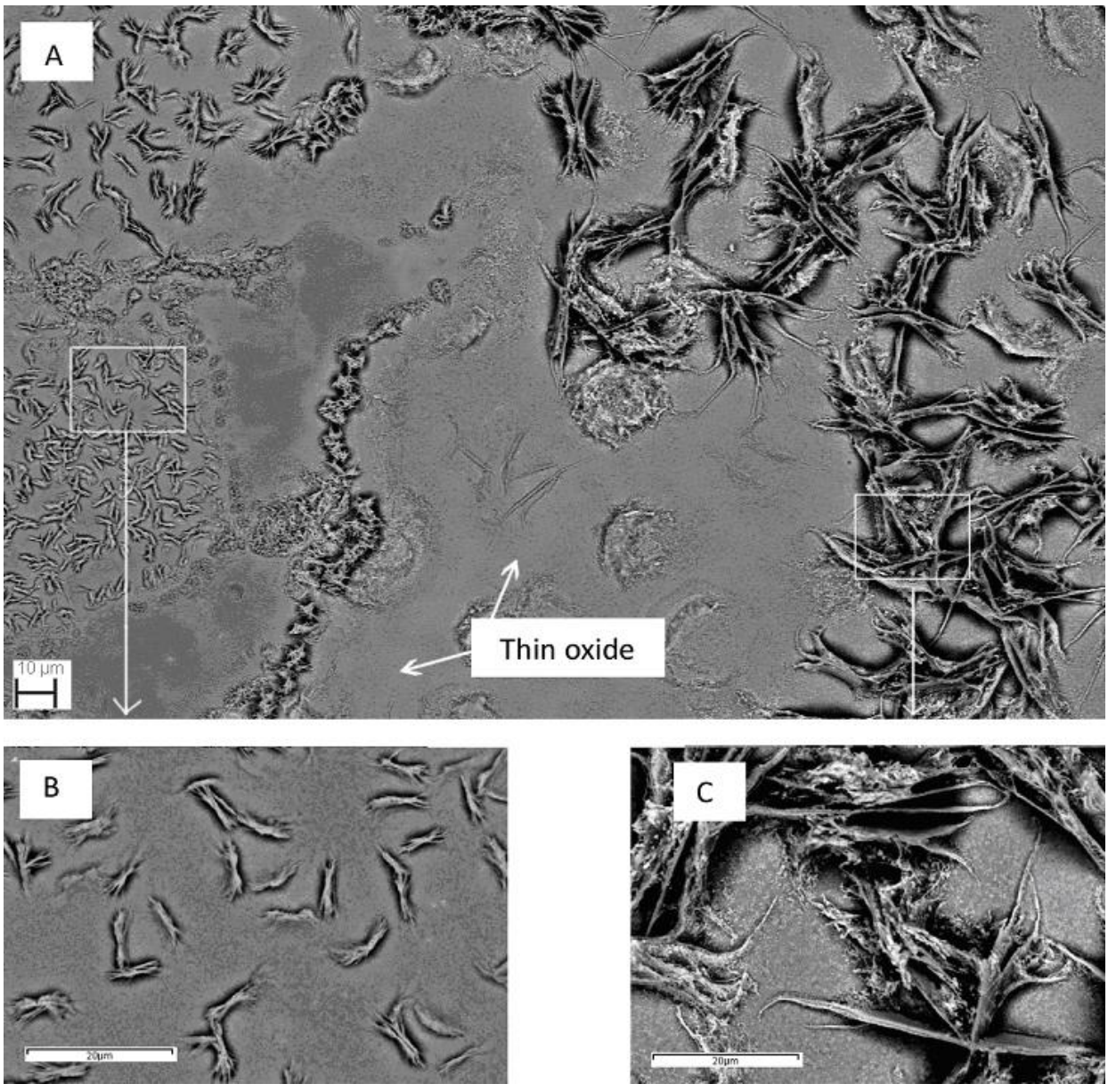

Figure 5.6. Fe-2.25Cr-1Mo in presence of $ZnCl_2$ at 300°C, 24h.

After 168 hours exposure, many diffuse, small formations appear as seen in *figure 5.7*, with a composition matching Fe_2ZnO_4 and ZnO. The small formations after 24 hours exposure (*figure 5.6 B*) still remain, but with more diffuse outlines, partly caused by a thicker layer of base oxide consisting of iron oxide. EDX showed that the oxide contained less Zn (~15%) compared to corresponding 1 and 24 exposures. As after 1 and 24 hours, no Cl was detected.

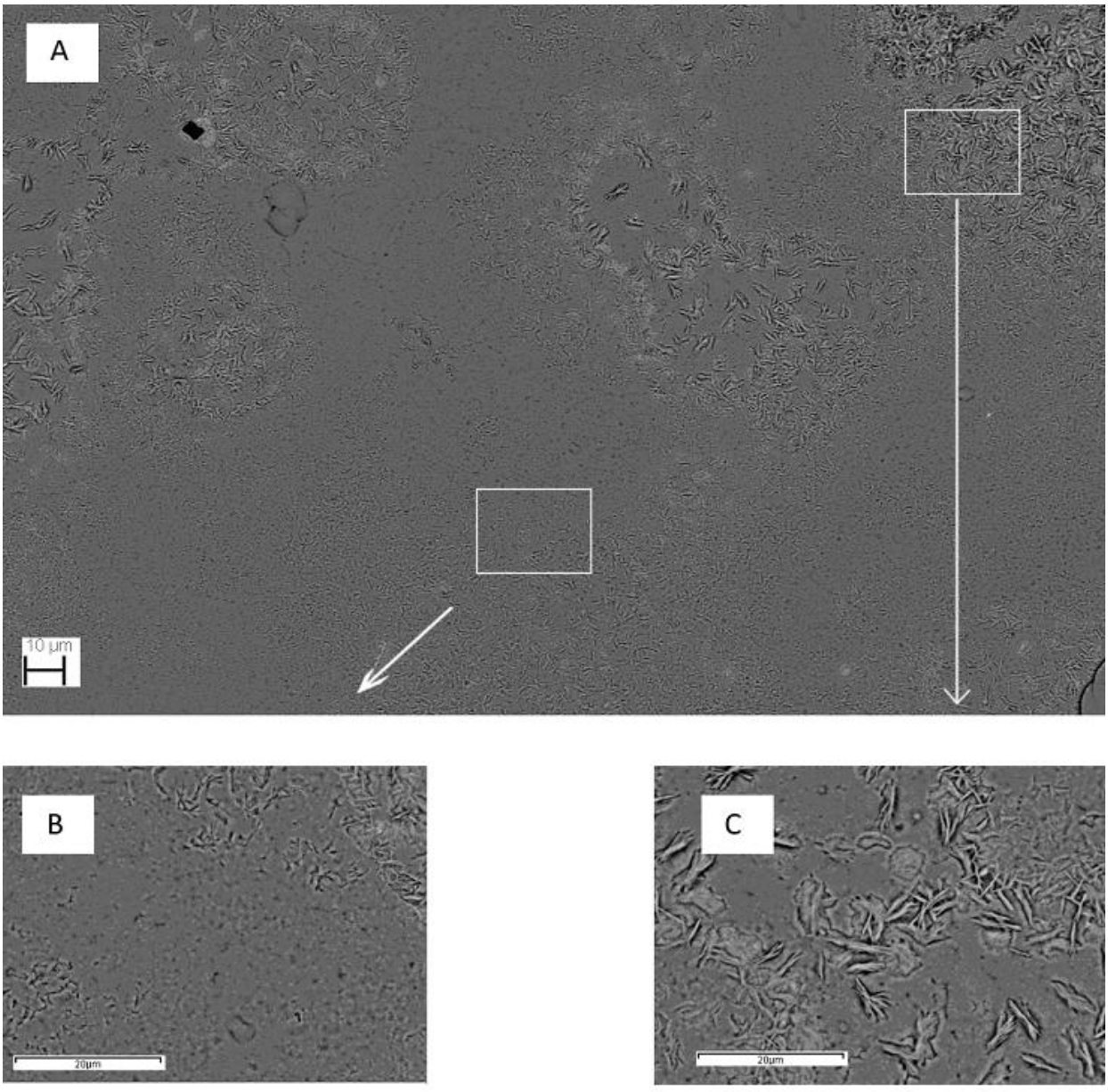

Figure 5.7. Fe-2.25Cr-1Mo in presence of $ZnCl_2$ at 300°C, 168h.

5.3 Oxidation of Fe-2.25Cr-1Mo in presence and absence of $ZnCl_2$ at 400 °C

5.3.1 Mass change

Figure 5.8 shows mass gain up to 168 hours. During reference exposures at 400°C, without $ZnCl_2$, a modest mass gain was observed. The oxide kinetics approximatley follows a parabolic oxidation rate growth at 300ºC.

It is clear that the presence of $ZnCl_2$ induces a significantly faster oxidation rate resulting in a higher mass gain compared to the reference. In presence of $ZnCl_2$, the curve shows a parabolic oxidation rate. During the first 24 hours, the oxidation rate is rather fast but then levels off.

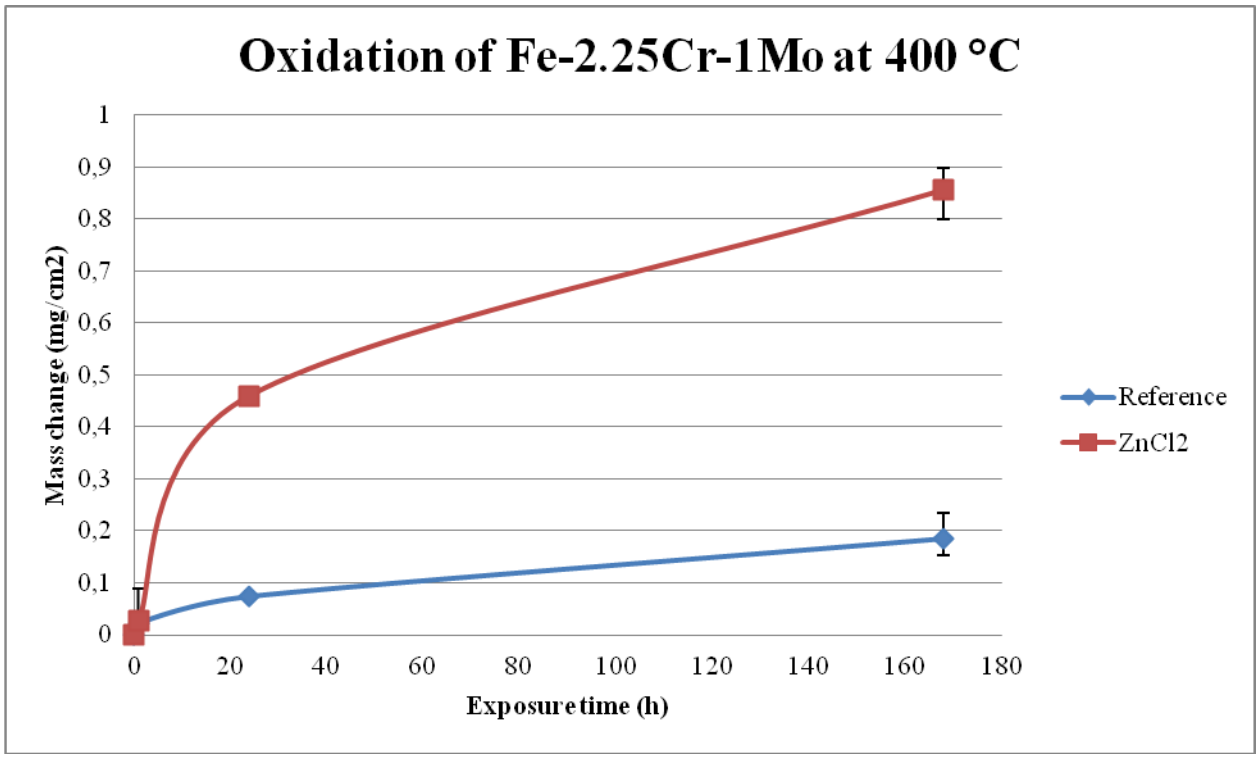

Figure 5.8. Mass change curve of Fe-2.25Cr-1Mo in both absence and presence of $ZnCl_2$.

5.3.2 Oxide morphology at 400°C

In absence of $ZnCl_2$: At high magnification, a smooth homogenous oxide growth is clearly observed. The oxide blades grow larger after time (*see figure 5.9*). After 1, 24 and 168 hours the oxide thickness was calculated to 44, 142 and 356 nm respectively.

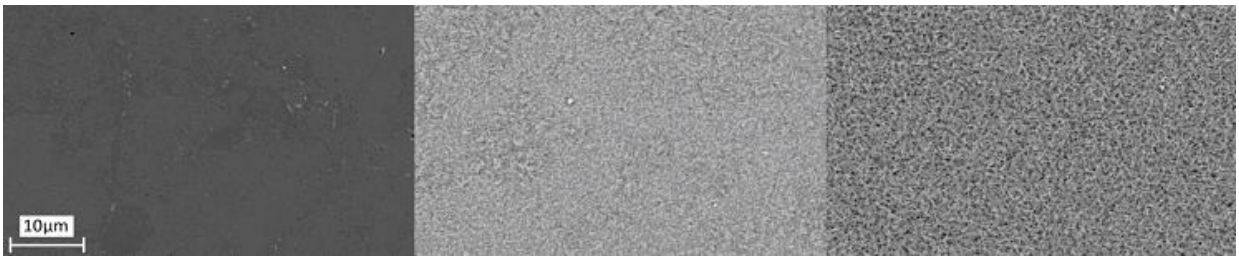

Figure 5.9. Reference samples of Fe-2.25Cr-1Mo at high magnification after 1, 24, 168 h.

In presence of $ZnCl_2$: After 1 hour exposure, a smooth base oxide covers the parts between the former salt deposits. According to EDX, the former salt deposits of Zn (28%), Fe (12%) and O (60%). No Cl was detected. A characteristic morphology can be seen in *figure 5.10 B.*

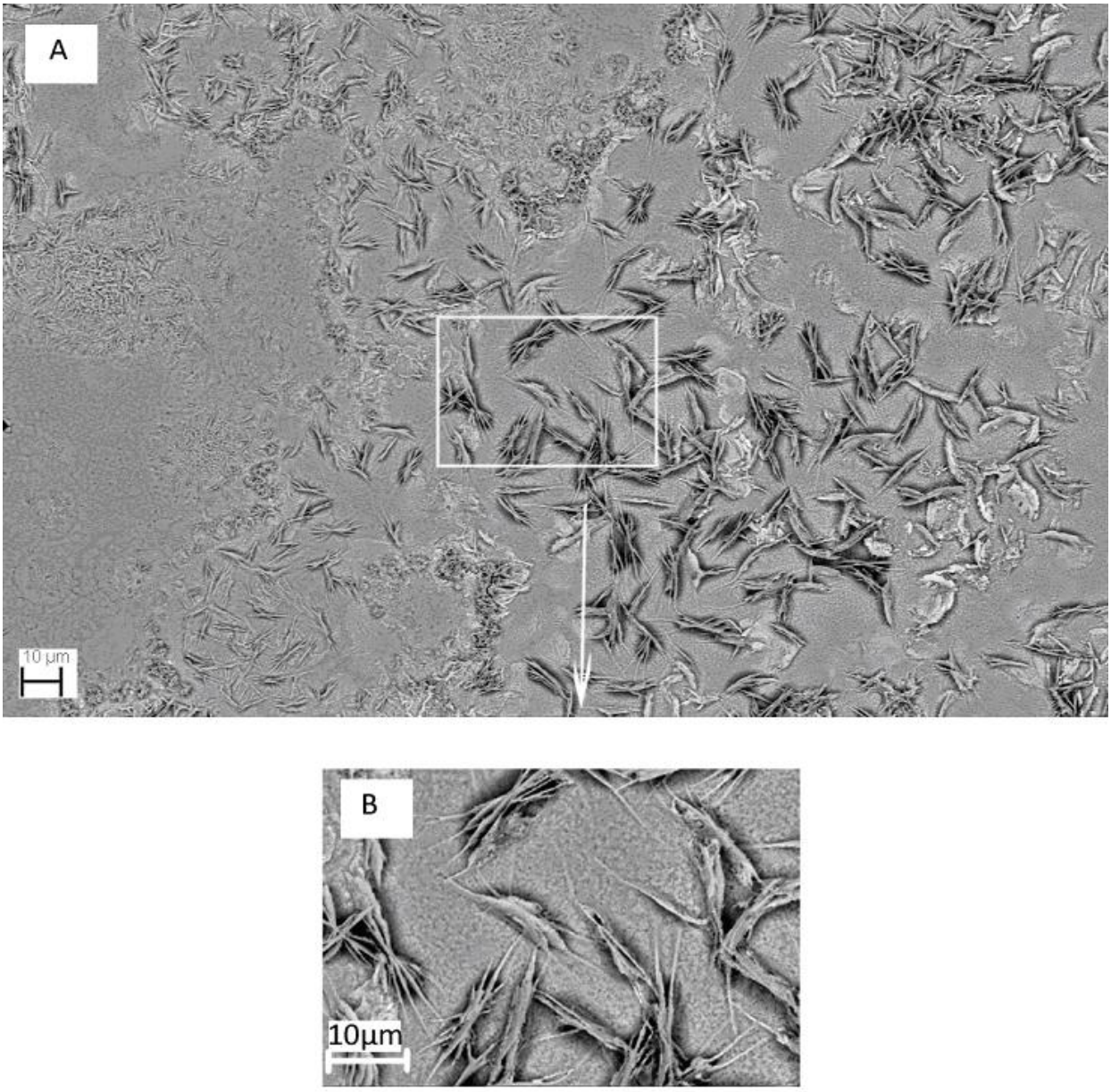

Figure 5.10. Fe-2.25Cr-1Mo in presence of $ZnCl_2$ at 400°C, 1h.

After 24 hours, a smooth base oxide covers the parts between the salt deposits. Characteristic oxide formations shown in *figure 5.11 B* have an average size of 10 – 20 µm. The brighter areas shown in *figure 5.11 C* contain ~ 60% O, 25% Zn and 15% Fe. The morphology seen in *figure 5.11 C* does not exist after 1 h.

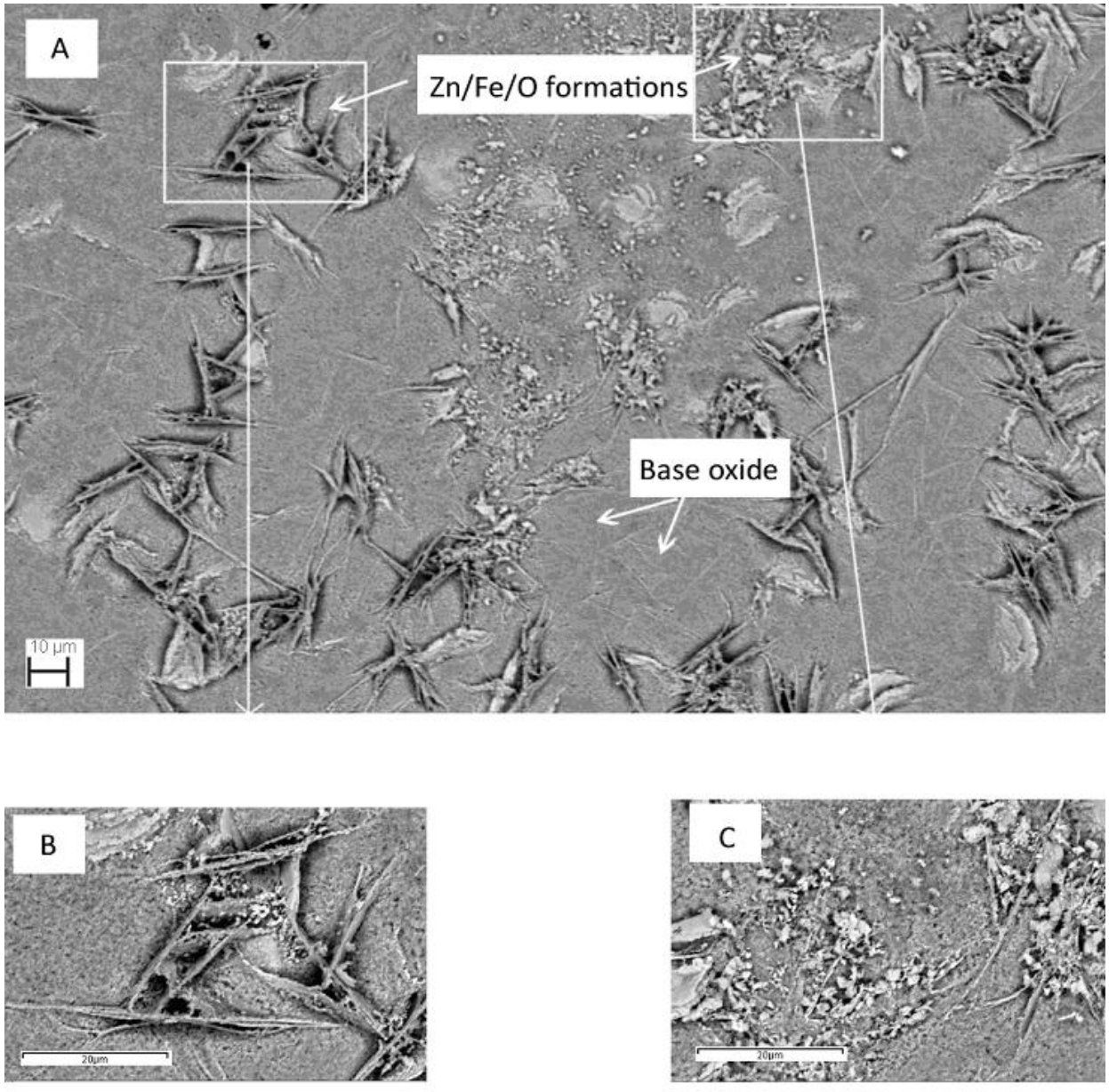

Figure 5.11. Fe-2.25Cr-1Mo in presence of $ZnCl_2$ at 400°C, 24h.

After 168 hours exposure, the base oxide whiskers are more visible (*see figure 5.12 B*) than after 24 h. According to XRD, the iron oxide consists of both hematite and magnetite. Sharp zinc and iron containing formations with an average size of 10-15 µm are mixed with more diffuse formations, similar to both 1 and 24 h exposure. No Cl was detected.

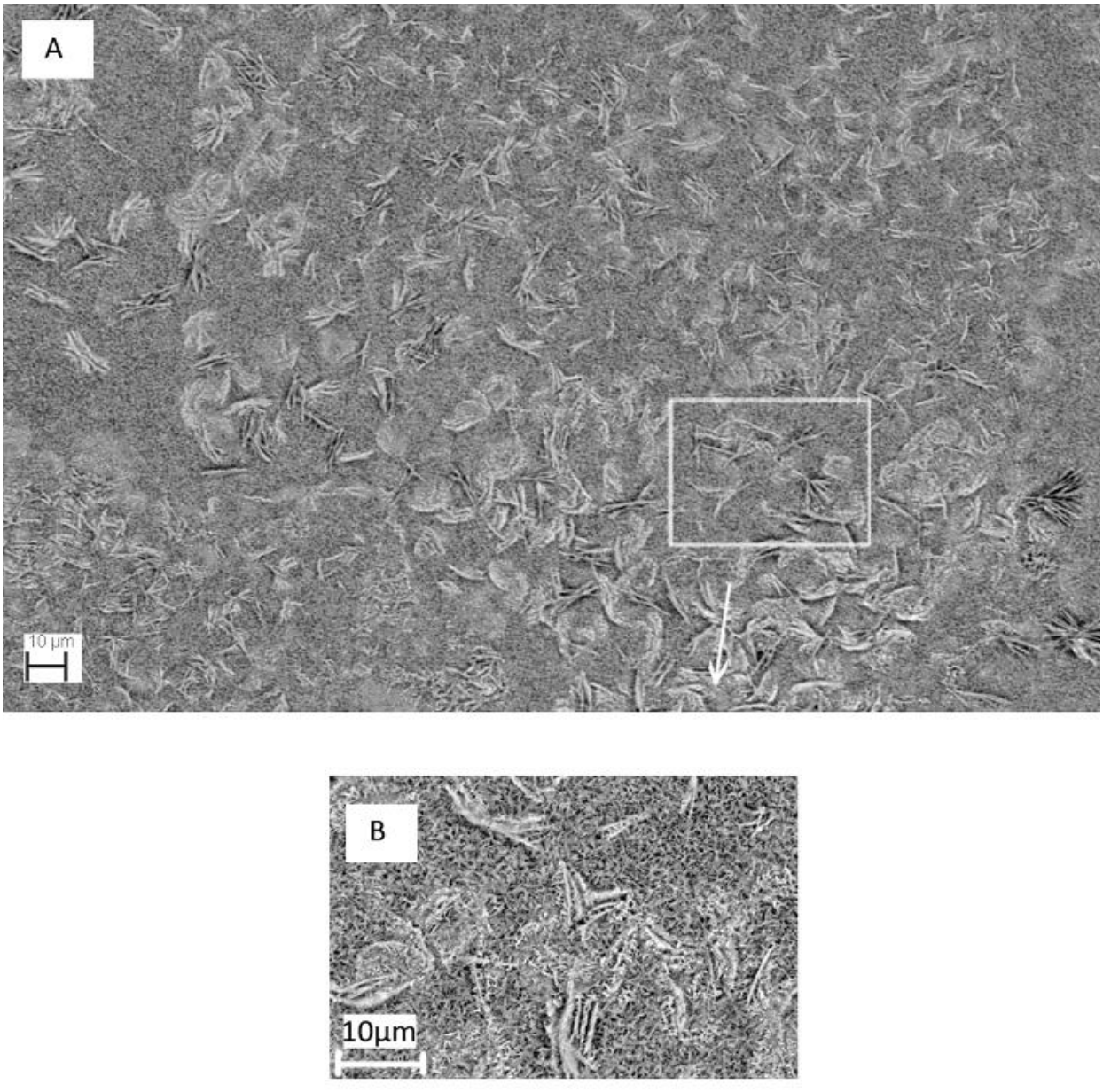

Figure 5.12. Fe-2.25Cr-1Mo in presence of $ZnCl_2$ at 400°C, 168h.

6. Concluding discussion

This thesis investigates the effect of $ZnCl_2$ in high temperature corrosion of low alloyed steels at 300 and 400°C. The experiments were carried out in a controlled environment yielding similar morphologies of the corrosion products at both temperatures. Since $ZnCl_2$ is highly hygroscopic, reference tests were carried out on a Au plate to estimate the highest possible amount of ZnO yield by the deposited $ZnCl_2$ solution. Calculations of vapor pressure were performed at 427°C and 227°C (*appendix 10.1*) to make sure insignificantly low evaporation of $ZnCl_2$, but with evaporation of HCl according to *reaction a)*, p. 11. However, all experiments in this work were carried out at 300 and 400°C to simulate waterwalls conditions in a biomass fired boiler. Since the temperature is higher than 227°C, a higher evaporation rate has to be considered and was also confirmed by the results. In order to be able to compare the results with earlier investigations considering KCl, the same amount (0.1 mg pure salt/cm^2) had to be deposited. This was accomplished by the Au reference tests.

Reference tests of Fe-2.25Cr-1Mo without $ZnCl_2$ at 300 and 400°C were carried out in order to compare the effect of $ZnCl_2$. Exposures of Fe-2.25Cr-1M in absence were compared with samples in presence of $ZnCl_2$. The mass gain of the reference exposures showed a modest mass gain. The oxide kinetics behavior was approximately parabolic. In presence of $ZnCl_2$, the mass gain was significantly higher. Even though, it is difficult to estimate the oxide thickness due to the evaporation.

ZnO and iron oxides were formed as corrosion products. Also, the matching composition of the spinel Fe_2ZnO_4 was observed. This was confirmed by SEM/EDX and XRD. The SEM investigation confirmed that corrosion products formed by $ZnCl_2$ were concentrated to the deposits.

The mass change curve from exposures in presence of $ZnCl_2$ at 300°C (*figure 5.3*) shows a quick decline in mass after 1 hour, which can be explained by evaporation of $ZnCl_2$. Also the solvent is presumed to have evaporated, as may be seen by comparing SEM pictures of unexposed and exposed samples (*figure 7, 8*). First after 168 h exposure, the mass change is positive compared to reference test after 168 h. The overall low amounts of chlorine were also confirmed by EDX

measurements at longer exposures both at 300 and 400°C. The Au experiments with $ZnCl_2$ indicate that about 0.27 mg/cm^2 solvent is present at the start of each exposure. This will evaporate as H_2O. Considering this, the mass gain due to oxidation would be about 0.27 mg/cm^2 higher.

Reference exposures as well as exposures in presence of $ZnCl_2$ at 400°C show a parabolic oxide growth, which declines after 24 h. Compared to reference exposures at 300°C, a thicker layer of base oxide was detected. After 168 h at 300 and 400°C in absence of $ZnCl_2$, the calculated base oxide thickness was 83 nm, 356 nm respectively (*figures 5.4, 5.9*).

For exposures at 400°C in presence of $ZnCl_2$, the mass change curve shows an immediate increase in mass (*figure 5.8*) in contrast to the mass loss at 300°C. Therefore, the evaporation rate of solvent and Cl is assumed to be much faster at 400°C and/or faster corrosion rate. Compared to reference at 400°C, the presence of $ZnCl_2$ significantly increases the oxidation rate. The same approximation as for 300°C can be made at 400°C considering the evaporation of approximately 0.27 mg/cm^2 H_2O. Considering this, the mass gain due to oxidation would be about 0.27 mg/cm^2 higher.

Already after 1 h at 300°C, zinc oxide and very low amounts of chlorine were detected, indicating a very fast reaction and no signs of $ZnCl_2$ melts could be detected. Compared to previous studies of KCl, a higher amount of Cl could be detected after exposures in presence of KCl. This is related to thermodynamics. According to calculations of the partial pressure of HCl (pHCl) at 300°C formed from $ZnCl_2$ is 0.00168 bar and KCl is $2.78 \cdot 10^{-8}$ bar. The differences in partial pressure explain why much lower amounts of Cl was detected even after short exposure times and low temperatures.

In biomass fired boilers, $ZnCl_2$ deriving from the fuel could condense on the waterwalls to form melt, which is suggested to induce corrosion. This introductory investigation considering $ZnCl_2$ is similar to the corrosion behavior of KCl, which does not form a melt at these temperatures. Between 24 and 168h exposure, the relative mass gain caused by $ZnCl_2$ and KCl regardless evaporation of H_2O is approximately the same. However, further investigations have to be carried out to better understand the role of $ZnCl_2$ in biomass fired boilers on low alloyed steels.

7. Proposal to further investigation

This thesis gives an overview of the oxidation of Fe-2.25Cr-1Mo by $ZnCl_2$ at 300 and 400°C. From both gravimetry and SEM it is clear that $ZnCl_2$ dramatically increases the corrosion rate. However, to gain deeper understanding, other analysis methods like Broad Ion Beam (BIB) could be helpful to study the microstructure of the corrosion scale in cross section.

In this study, the amount of salt sprayed on the samples has been held approximately constant at each exposure. However, it would be interesting to vary the amount of salt deposit to compare the amount of salt with the corrosion rate.

Pure $ZnCl_2$ has a melting point at approximately 300°C. In a biomass fired boiler, there are many mixtures of different salts. For example, the mixture of $ZnCl_2$ and KCl has a melting point at about 230°C. Hence, it will induce corrosion at an earlier stage than pure $ZnCl_2$. Therefore, mixtures of $ZnCl_2$ and KCl in different proportions could be of interest to investigate.

Finally, to compare different heavy metals and their influence of corrosion, for example $PbCl_2$, could be investigated to see the difference between heavy metals containing chlorine.

8. Acknowledgements

This work was carried out at The Swedish High Temperature Corrosion Centre (HTC) at Chalmers University of Technology, Gothenburg Sweden.

First of all, we would like to thank our examiner Professor Jan-Erik Svensson for making this project possible.

We would also like to thank Professor Lars-Gunnar Johansson for sharing his expertise in high temperature corrosion.

Furthermore, we would like to express our great appreciation to our supervisor Torbjörn Jonsson Ph. D., who has supported us from start to finish. Torbjörn has shown true commitment in the research subject and also in helping us in many different ways.

We would also like to thank our other supervisor Erik Larsson Ph. D Student, who taught us many practicalities as well as supported us in our work.

Moreover, we would like to thank Jesper Pettersson Ph. D., for his expertise, interesting discussions and problem solving.

Finally, we would like to send our thankfulness to all the rest of the personnel at HTC, who have showed kindness and made us feel welcome.

Patrik Åkesson & Gustaf Ålander

Gothenburg 30/5-2011

9. References

1. Vainikka P., Bankiewich D., Frantsi A., Silvennionen J., Hannula J., Yrjas P., Hupa M. (2011) *High temperature corrosion of boiler waterwalls induced by chlorides and bromides. Part 1: Occurrence of the corrosive ash forming elements in a fluidised bed boiler co-firing solid recovered fuel pp. 2055-2056*, Jyväskulä: Elsevier Ltd
2. Naturvårdsverket (2011). *Reduced Climate Impact*. http://miljomal.se/Environmental-Objectives-Portal/1-Reduced-Climate-Impact/ (31 March 2011)
3. Zumdahl S.S. (2005) *Chemical Principles p. 383*, Fifth edition. Boston: Houghton Mifflin Company
4. Henderson P.J., Andersson C., Kassman H., Högberg., Szakálos P., Pettersson R. (2008) *Novel Approaches to Improving High Temperature Corrosion Resistance EFC 47 p. 428*, Woodhead Publishing
5. Li Y.S., Niu Y., Wu W.T. (2002) *Accelerated corrosion of pure Fe, Ni, Cr and several Fe-based alloys induced bu ZnCl2-KCl at 450 °C in oxidizing environment p. 64*, Elsevier Science B. V.
6. Vainikka P., Bankiewich D., Frantsi A., Silvennionen J., Hannula J., Yrjas P., Hupa M. (2011) *High temperature corrosion of boiler waterwalls induced by chlorides and bromides. Part 1: Occurrence of the corrosive ash forming elements in a fluidised bed boiler co-firing solid recovered fuel pp. 2055-2056*, Jyväskulä: Elsevier Ltd
7. Folkeson N. (2010) *Chlorine Induced Corrosion in Biomass and Waste Fired Boilers: Laboratory and Field Investigations p. 12*, in Department of Chemical and Biological Engineering. Gothenburg: Chalmers University of Technology
8. Zumdahl S.S. (2005) *Chemical Principles pp. 784-785*, Fifth edition. Boston: Houghton Mifflin Company
9. Talbot S. (2007) *Corrosion Science and Technology pp. 117, 118, Second edition*. Boca Raton: Taylor & Francis Group
10. Ohring M. (1992) *Materials Science of Thin Films – Deposition and Structure pp. 10-13*, San Diego: Academic Press

11. Folkeson N. (2010) *Chlorine Induced Corrosion in Biomass and Waste Fired Boilers: Laboratory and Field Investigations p. 17*, in Department of Chemical and Biological Engineering. Gothenburg: Chalmers University of Technology
12. Folkeson N. (2010) *Chlorine Induced Corrosion in Biomass and Waste Fired Boilers: Laboratory and Field Investigations pp. 18-20*, in Department of Chemical and Biological Engineering. Gothenburg: Chalmers University of Technology
13. Folkeson N. (2010) *Chlorine Induced Corrosion in Biomass and Waste Fired Boilers: Laboratory and Field Investigations p. 16*, in Department of Chemical and Biological Engineering. Gothenburg: Chalmers University of Technology
14. Pettersson J. (2008) *Alkali Induced High Temperature Corrosion of Stainless Steel, Experiences from Laboratory and Field, pp. 6, 7*, in Department of Chemical and Biological Engineering. Gothenburg: Chalmers University of Technology
15. Talbot S. (2007) *Corrosion Science and Technology pp. 117, 118, Second edition*. Boca Raton: Taylor & Francis Group
16. Pettersson J. (2008) *Alkali Induced High Temperature Corrosion of Stainless Steel, Experiences from Laboratory and Field, pp. 6-9*, in Department of Chemical and Biological Engineering. Gothenburg: Chalmers University of Technology
17. Talbot S. (2007) *Corrosion Science and Technology p. 119, Second edition*. Boca Raton: Taylor & Francis Group
18. Folkeson N. (2010) *Chlorine Induced Corrosion in Biomass and Waste Fired Boilers: Laboratory and Field Investigations pp. 18-20*, in Department of Chemical and Biological Engineering. Gothenburg: Chalmers University of Technology
19. Folkeson N. (2010) *Chlorine Induced Corrosion in Biomass and Waste Fired Boilers: Laboratory and Field Investigations pp.23-24*, in Department of Chemical and Biological Engineering. Gothenburg: Chalmers University of Technology
20. Aylward G., FindlayT., (2002) *SI Chemical Data pp. 62, 86, Fifth edition*. Milton: John & Wiley & Sons Australia
21. Vainikka P., Bankiewich D., Frantsi A., Silvennionen J., Hannula J., Yrjas P., Hupa M. (2011) *High temperature corrosion of boiler waterwalls induced by chlorides and bromides. Part 1: Occurrence of the corrosive ash forming elements in a fluidised bed boiler co-firing solid recovered fuel pp. 2055-2056*, Jyväskulä: Elsevier Ltd

22. Folkeson N. (2010) *Chlorine Induced Corrosion in Biomass and Waste Fired Boilers: Laboratory and Field Investigations pp. 29-30*, in Department of Chemical and Biological Engineering. Gothenburg: Chalmers University of Technology
23. Folkeson N., Jonsson T., Halvarsson M., Johansson L.-G., Svensson J.-E. (2010) *The influence of small amounts of KCl(s) on the high temperature corrosion of a Fe-2.2Cr-1Mo steel at 400 and 500°C.* Weinheim: WILEY-VCH Verlag GmBH & Co. KGaA
24. Goldstein J. I., Romig Jr, A. D., Newbury D. E., Lyman C. E., Echlin P., Fiori C., Joy D. C., Lifshin E. (1992) *Scanning Electron Microscopy and X-Ray Microanalysis pp. 1, 21-24,69,95,Second edition*. New York: Plenum Press
25. Zumdahl S.S. (2005) *Chemical Principles pp. 771-774*, Fifth edition. Boston: Houghton Mifflin Company
26. Atkins P., De Paula J. (2006) *Atkins' Physical Chemistry pp. 702-704, 8th edition*. Oxford: Oxford University Press

10. Appendix

10.1 Calculations of vapor pressure for $ZnCl_2$ at 700K and 500K

10.1.1 Calculation of vapor pressure for $ZnCl_2$ at 700K

Presume the following equilibrium reaction:

$$ZnCl_{2\,(s)} \leftrightarrow ZnCl_{2\,(g)}$$

$\Delta G_{f\,(700K)}$ for reaction above is +34,723 kJ/mol.

Equilibrium constant in terms of partial pressure:

$$K_p = \frac{p(ZnCl_2)}{a(ZnCl_2)_{(s)}} = p(ZnCl_2)_{(g)}$$

Equilibrium constant calculated from difference in Gibbs free energy at given temperature.

$$K = \exp\left(\frac{-\Delta G_f}{RT}\right)$$

Vapor pressure for $ZnCl_2$ at 700K is calculated as followed:

$$\frac{K_p(700) = p(ZnCl_2)_{(g)} = \exp(-34723)}{(8{,}314 \cdot 700)} = \exp(5{,}966) = 2{,}56 \cdot 10^{-3}\ \mathbf{bar}$$

10.1.2 Calculation of vapor pressure for $ZnCl_2$ and HCl at 500K

Presume the following equilibrium reaction:

$$ZnCl_{2\,(s)} + H_2O_{\,(g)} \rightarrow ZnO_{\,(s)} + 2HCl_{\,(g)}$$

$\Delta G_{f\,(500K)}$ for reaction above is +63,61 kJ/mol.

Equilibrium constant in terms of partial pressure:

$$K_p = \frac{(pHCl)^2 \cdot aZnO_{(s)}}{aZnO_{(s)} \cdot pH_2O} = \frac{(pHCl)^2}{pH_2O}$$

Vapor pressure for $ZnCl_2$ at 500K is calculated as followed:

$$K_p(500) = pZnCl_{2(g)} = \exp\left(\frac{-63610}{(8{,}314 \cdot 500)}\right) = \exp(-15{,}30) = 2{,}26 \cdot 10^{-7} bar$$

Vapor pressure for HCl at 500K:

$$pHCl = \sqrt{K \cdot pH_2O} = \sqrt{2{,}26 \cdot 10^{-7} \cdot 0{,}4} = \sqrt{9{,}05 \cdot 10^{-8}} = pHcl(500) = 3 \cdot 10^{-4}$$ bar

10.2 Amount of formed ZnO (s) and amount of belayed $ZnCl_2$ (s) per cm^2 on sample coupons

Equilibrium reaction

$ZnCl_{2\ (s)} + H_2O_{\ (g)} \rightarrow ZnO_{\ (s)} + 2HCl_{\ (g)}$

Test 1

Oxidation of $ZnCl_2$ into ZnO at 227 °C (500K) on a 0.63 cm^2 Au coupon

Weight before exposure (g):	2.6013965
Weight after spraying (g):	2.601602
Weight after exposure (g):	2.601484

Amount of belayed $ZnCl_2$ = 2.601602 - 2.6013965 = 206 µg

Amount of ZnO = 206 µg - (2.601484 – 2,6013965) = 119 µg

Calculation of moles ZnO.

Mass ZnO = 119 µg

Molar mass ZnO = 81,38 g/mol

Mole ZnO = 0,00968422

Presume that mole ZnO equals to mole $ZnCl_2$.

Mole $ZnCl_2$ = 0,00968422

Molar mass $ZnCl_2$ = 136,315 g/mol

Mass $ZnCl_2$ = 710,43 µg

Area Au coupon = 0,63 cm^2

Amount $ZnCl_2$ = 0,1128 mg/cm^2

Test 2

Oxidation of $ZnCl_2$ into ZnO at 227 °C (500K) on a 0.63 cm^2 Au coupon

Weight before exposure (g): 2,6013605

Weight after spraying (g): 2,601506

Weight after exposure (g): 2,601429

Amount of belayed $ZnCl_2$ = 2,601506 - 2,6013605 = 145 µg

Amount of ZnO = 145 µg - (2,601429 – 2,6013605) = 77 µg

Calculation of moles ZnO

Mass ZnO = 77 µg

Molar mass ZnO = 81,38 g/mol

Mole ZnO = 6,27E-03

Presume that mole ZnO equals to mole $ZnCl_2$.

Mole $ZnCl_2$ = 6,27E-03

Molar mass $ZnCl_2$ = 136,315 g/mol

Mass $ZnCl_2$ = 4,60E-05 g

Area Au coupon = 0,63 cm^2

Amount $ZnCl_2$ = 0,073 mg/cm^2

Average cover of $ZnCl_2$ = 0,093 mg/cm^2

10.3 Temperature profiles

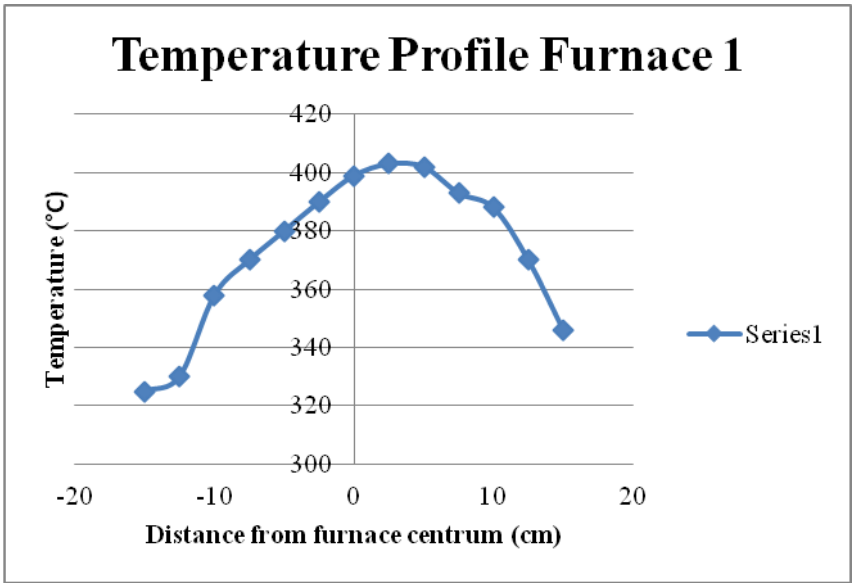

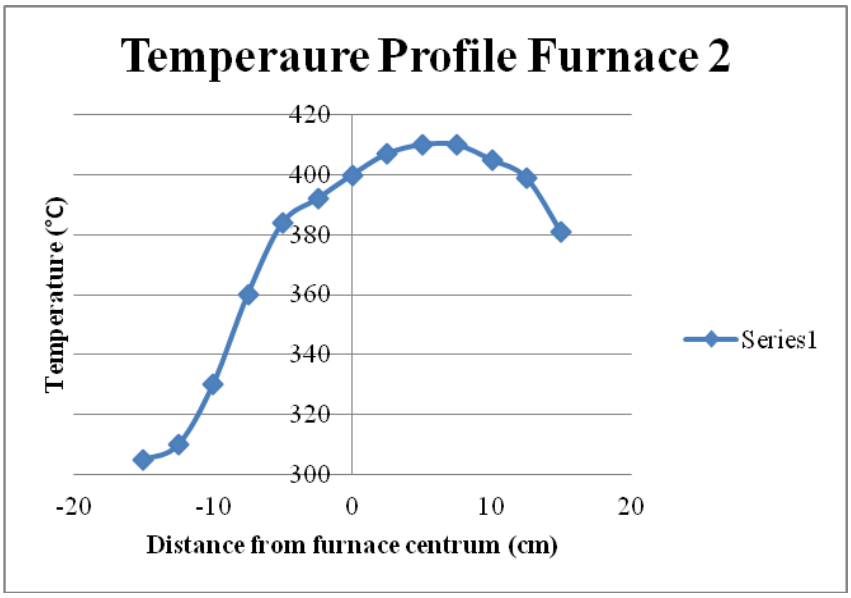

10.4 Example of EDX composition measurements

10.4.1 T22, 300 °C, 168h in presence of $ZnCl_2$

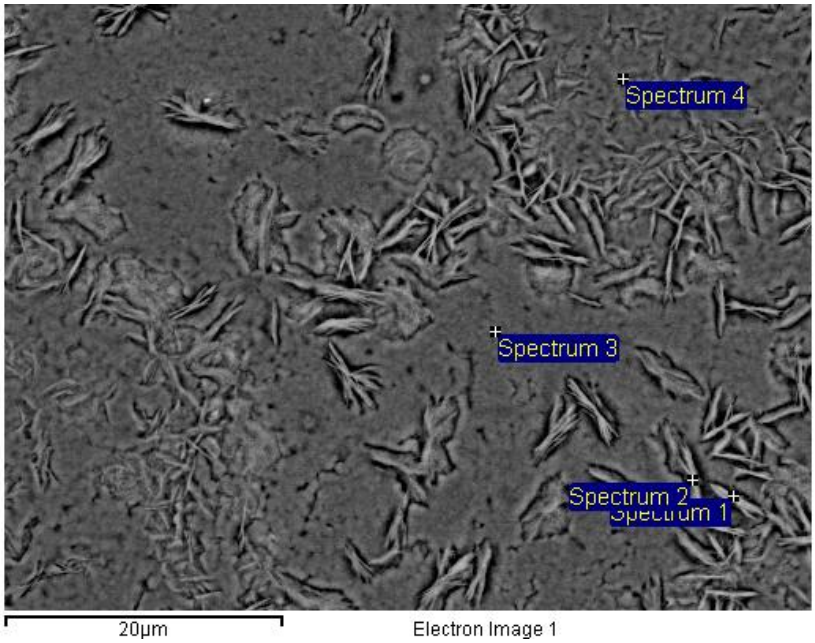

Spectrum	In stats.	O	Si	Cl	Cr	Mn	Fe	Zn	Mo
Spectrum 1	Yes	63.25	2.96	0.51	0.22	0.07	17.93	15.04	0.03
Spectrum 2	Yes	47.89	2.85	0.52	0.40	0.18	32.14	15.95	0.08
Spectrum 3	Yes	59.29	1.98	0.17	0.72	0.19	36.43	1.11	0.12
Spectrum 4	Yes	60.11	2.19	0.21	0.78	0.18	35.20	0.86	0.47
Mean		57.63	2.49	0.35	0.53	0.15	30.42	8.24	0.18
Std. deviation		6.72	0.48	0.19	0.27	0.06	8.53	8.39	0.20
Max.		63.25	2.96	0.52	0.78	0.19	36.43	15.95	0.47
Min.		47.89	1.98	0.17	0.22	0.07	17.93	0.86	0.03

All results in atomic%

10.4.2 T22, 400 °C, 168h in presence of $ZnCl_2$

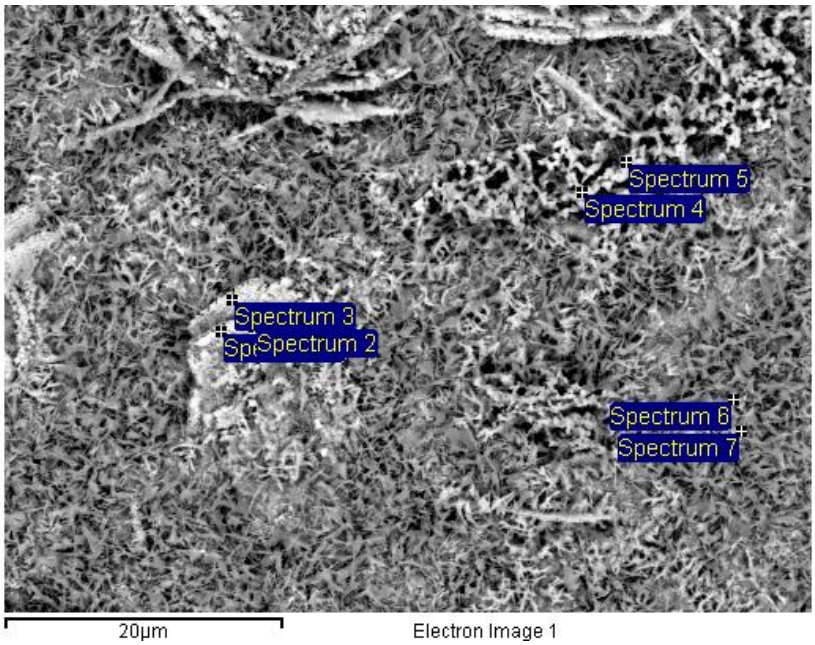

Spectrum	In stats.	O	Si	Cl	Cr	Mn	Fe	Zn	Mo
Spectrum 1	Yes	58.02	0.28	0.74	-0.03	0.12	11.13	29.72	0.02
Spectrum 2	Yes	56.33	0.27	0.70	0.11	0.11	15.56	26.93	0.01
Spectrum 3	Yes	64.21	0.16	0.32	0.13	0.11	18.13	16.92	0.02
Spectrum 4	Yes	60.36	0.21	0.55	0.18	0.15	24.47	14.08	0.02
Spectrum 5	Yes	52.63	0.12	0.18	0.23	0.23	42.11	4.50	-0.01
Spectrum 6	Yes	57.94	0.13	-0.01	0.17	0.28	40.47	1.01	0.00
Spectrum 7	Yes	61.77	0.10	0.01	0.18	0.27	37.18	0.47	0.02
Mean		58.75	0.18	0.36	0.14	0.18	27.01	13.38	0.01
Std. deviation		3.79	0.07	0.31	0.09	0.08	12.79	11.99	0.01
Max.		64.21	0.28	0.74	0.23	0.28	42.11	29.72	0.02
Min.		52.63	0.10	-0.01	-0.03	0.11	11.13	0.47	-0.01

All results in atomic%